Summary. A major part of the SECC purview is to determine the levels of past and future shaking from strong earthquakes. We concentrated on the effects of major earthquakes on the San Andreas Fault on sedimentary basins, including those beneath Los Angeles. Numerical modeling by the SECC community and the reports of the 1857 earthquake indicate that these earthquakes produce surface waves (mostly Love waves with horizontal motion) that reverberate within the basin for 1 to 2 minutes and that the dominant period of these waves is 3-4 seconds. These waves produce dynamic stress in the Earth through which these propagate. Shallow (upper few hundred meters) rocks fail in friction when the dynamic stress exceeds the pressure of the overlying rock minus pore-water pressure times the coefficient of friction. The dynamic stress is simply the ground velocity divided by the (phase) velocity of wave propagation times the shear modulus. A shallow seismic regolith of cracked rock self-organizes over several earthquake cycles. Initially stiff rock cracks reducing its shear modulus, eventually to the point that cracking barely occurs at peak stress. The shallow shear modulus then increases linearly with depth, which is observed. The water table in basins within Los Angeles was likely near the surface in the 1857 and earlier events. The observed increase of shear modulus with depth indicates peak ground velocities of 0.3 to 1.6 meter per second in past events at various sites. That is, shallow rock is a fragile geological feature that is conveniently ubiquitous. In addition, shaking greater than these levels would crack the rock, sapping energy from the waves as they cross the basins. These levels thus provide limits on future shaking. In detail the water table is now deeper than in 1857, about 60 m beneath downtown Los Angeles. This drawdown, however, increases the maximum amplitude of waves that can propagate by only 10%. These peak ground velocity values from analysis of shear modulus are in range obtained by the SECC community for shaking within Los Angeles. That is, nonlinear attenuation is likely important around Los Angeles and within other similar basins. SECC community numerical methods and methods based on ambient noise seismology assume linearity and need to be modified. Semi-empirical site response methods are inadequate since nonlinear attenuation saps surface waves along their full path. Our intent is to do two-dimensional calculations for Love waves to develop the formalism so that it can be included in sophisticate SECC community models. The results will need to be eventually appraised with strong motion data in sedimentary basins.

We numerically modeled the simple one-dimensional case of a vertically propagating shear wave to gain insight into the more complicated case of surface waves. Real rock is likely to have numerous fractures, some with pre-existing stress, that fail over a range of dynamic stresses. We obtained a convenient way to include this effect in our calculations. The computed velocity seismogram is saw-toothed. The constant acceleration legs of the curve in g's are approximately the apparent coefficient of friction. We obtained an apparent coefficient of friction of 0.4 near Parkfield for the 2004 event, which is approximate for a shallow water table at the site.

We continued other work relevant to failure of shallow rocks, including the "lid" region of blind faults, Archean seismic regolith from an asteroid impact, and regolith from tidal stress on moons of giant planets. We examined the Lucerne record of the Landers earthquake for nonlinear effects. We obtained a constraint on the recurrence of outer-rise earthquakes off Japan. The Central Valley is analogous but recurrence is a factor of 30 lower. We also studied rate and state friction for application to shallow rocks.

Technical report. We concentrated on shallow processes for the practical applications of exceedance and nonlinear attenuation. Intact rock and seismically damaged regolith are long-lasting fragile ubiquitous geological features. We developed formalism for nonlinear attenuation of strong S-waves. We are studying the societal problem of nonlinear behavior of strong Love waves within sedimentary basins, including those in the Los Angeles area that is central to SCEC's purview.

Outreach work: Other examples of shallow rock damage. We remained alert for other implications of near-surface rock damage. (1) We examined the Lucerne seismic record near the Landers earthquake fault to search for transient damage. The data proved unsuitable. We recovered the "lost" vertical component from an eps plot file and showed that vertically reverberating P-waves caused a broad resonance. Other broad resonances exist on the horizontal components. The seismic source was not especially rich in high frequencies [1]. (2) We obtained working numerical models for the lids of blind faults as proposed last year. Lids with long-term ductile material will self organize if the Maxwell time (shear modulus/viscosity) is comparable to the earthquake cycle time. Damage from repeated events makes the lid more compliant and co-seismically elastic [2]. Significant co-seismic distributed brittle dilatation occurred in the lid at Bam [3], using [4-6], comparable long-term ductile strain is permissible. (3) Don Lowe has found Archean seismic regolith from extreme seismic waves from impact of a ~50 km diameter asteroid at a distance of 10s of degrees. We have scaling relationships for Rayleigh and P waves. Tidal regolith analogous to seismic regolith likely forms on Saturn's moon Enceladus and on rocky bodies is a habitable environment [7]. Ground truth wherever obtained is useful to our gross problem. (4) We published brief paper on the likelihood of great outer-rise earthquakes associated with the Tohuku mainshock [8]; its results can be extrapolated to flexure in the Central Valley. (5) We studied physical basis of hybrid rate and state friction laws [9] using data from [10]. For attenuation and damage studies, the slip law [11] applies at the start of slip and rapid dilatation occurs at low normal tractions. This concept is closely related to the construct of dilatancy angle in engineering [4-6].

Societal and technical results on nonlinear attenuation. Strong seismic waves pass through the shallow (10s to 100s of m) subsurface. These ambient rocks fail in a brittle manner and become cracked. This process transiently reduces the low-amplitude seismic velocity of the damaged rocks. Over time, damage accumulates reducing the low-amplitude seismic velocity below that of intact rock. Rock damage self-organizes over providing both exceedance criteria for past strong motions and for future motions of the strongest waves that can propagate without significant nonlinear attenuation [12]. For explanation, we start seismic cycles with stiff exhumed sedimentary rocks extending all the way to the surface. We obtained the shallow failure criterion relevant to Los Angeles by noting that Love waves impose essentially strain boundary conditions on the shallow subsurface. The peak dynamic strain is V_0/c_L where V_0 is peak ground velocity and c_L is phase velocity. The dynamic shear traction on vertical planes is $G(z)V_0/c_L$, where $G(z)$ is the shear modulus at a depth z. Coulomb failure occurs when the dynamic stress exceeds the frictional strength $G(z)V_0/c_L = \rho\beta^2(z)V_0/c_L = \rho\mu_{\text{eff}}gz$, where ρ is density (here constant for simplicity), $\beta(z)$ is shear wave velocity, and μ is the intrinsic coefficient of friction. The final quality assumes that fluid pressure is hydrostatic $\rho_f gz$. Solving for shear wave velocity, the failure criterion is

$$\beta = \sqrt{c_L \mu_{\text{eff}} g z / V_0} \quad (1); \qquad \mu_{\text{eff}} \equiv (\rho - \rho_f)\mu / \rho, \quad (2)$$

where (2) defines an effective coefficient of friction for hydrostatic fluid pressure. If shaking is weak (low V_0), the S-wave velocity for failure exceeds the ambient velocity and the material stays linear. Otherwise Coulomb failure occurs during strong shaking with cracks that decrease the low-amplitude S-wave velocity. More cracks form in each strong event until the S-wave velocity approaches the failure criterion. Thereafter, the shallow subsurface barely becomes nonlinear in typical strong shaking. Conversely, waves from a rogue event with exceptionally large PGV would not propagate efficiently owing to nonlinear attenuation associated with Coulomb failure. Seismic velocity is observed to increase with depth as expected from (1) (Figure 1a) [12].

We modeled this nonlinear attenuation of strong S-waves to gain insight into the geometrically more complicated problem of basin Love waves. Our simple numerical method for vertically propagating S-waves in a constant velocity medium illustrates the general concept that Coulomb-based nonlinear attenuation clips acceleration so its peak in g's is the effective coefficient of friction. (P-waves clip only in tension at ~-1g [13-15].) Our group of adjacent displacement nodes is up (U), center (C), and down (D). The shear traction between two nodes (down and center) is

$$\tau(D,C) = G\left[\frac{U_{\text{down}} - U_{\text{center}}}{\Delta z}\right] - G\varepsilon(D,C), \quad (3); \qquad A_{\text{center}} = \frac{1}{\rho}\left[\frac{\tau(D,C) - \tau(C,U)}{\Delta z}\right]. \quad (4)$$

where the first term involves elasticity and $\varepsilon(D,C)$ is anelastic strain. The acceleration of the center node is given in (4). The gradient in stress at Coulomb failure is $\rho g \mu_{\text{eff}}$. The new velocity at the center node is then $V_{\text{new}} = V_{\text{old}} + A_{\text{center}} \Delta t$ and the new displacement is $U_{\text{new}} = U_{\text{old}} + V_{\text{new}} \Delta t$. Our method kinematically propagates waves through a linear elastic medium when $\Delta z / \Delta t = \beta$. The anelastic strain rate should be consistent with the stress:

$$\tau_{\text{new}} = G\left[\frac{U_{\text{down}} - U_{\text{center}}}{\Delta Z}\right] - G\varepsilon_{\text{old}} - G\Delta\varepsilon(\tau_{\text{new}}), \quad (5); \qquad \Delta\varepsilon = \left[\frac{\tau_M}{G}\right]\left[\frac{\tau_{\text{new}} - \tau_B}{\tau_M}\right]^M, \quad (6)$$

where $\Delta\varepsilon$ is the anelastic strain rate times the time step in a convenient function (6); $\tau_M = \rho g \mu_M z$ is a stress where frictional creep becomes fast at the Coulomb stress ratio μ_B; $\tau_B = \rho g \mu_B z$ implies that no creep occurs below a Bingham coefficient of friction of μ_B; and M (here 5) is an exponent that represents rapid transition between slow and fast deformation as dynamic stress increases. The stress τ_{new} appears on both sides of (5), which is readily solved by iteration. Equation (6) represents predictable deformation of a medium with various local pre-stresses where many randomly aligned fractures fail at different macroscopic stresses. It treats macroscopic rock failure as internal friction, without resolving individual crack failure, failure cascades, and their associated bursts of high-frequency signal.

Figure 2a shows a velocity pulse from the 2004 Parkfield mainshock. The waveform is saw-toothed with legs of nearly constant acceleration. The numerical model predicts this behavior for an incident sine wave (Figure 2b). The acceleration is clipped at high incident amplitudes, but the duration of high acceleration and hence PGV increase with incident amplitude (Figure 2c). The acceleration slope of the observed record ~0.4g is a measure of the effective coefficient of friction. Although detailed hydrology is not available, the water table was likely shallow. Assuming rock and fluid density of 2250 and 1000 kg/m^3 yields an intrinsic coefficient of friction in (2) of 0.72 compatible with

this inference. Our objective is to appraise and calibrate our methods for use with basin waves. Note that body waves in a highly stratified domain produce hard-to-interpret, ringy, high-frequency signal. High Coulomb stress ratios do occur in that case but only at very shallow depths. Such high-frequency signal often does not attenuate by Coulomb failure as very shallow rock has finite strength at zero normal traction (cohesion).

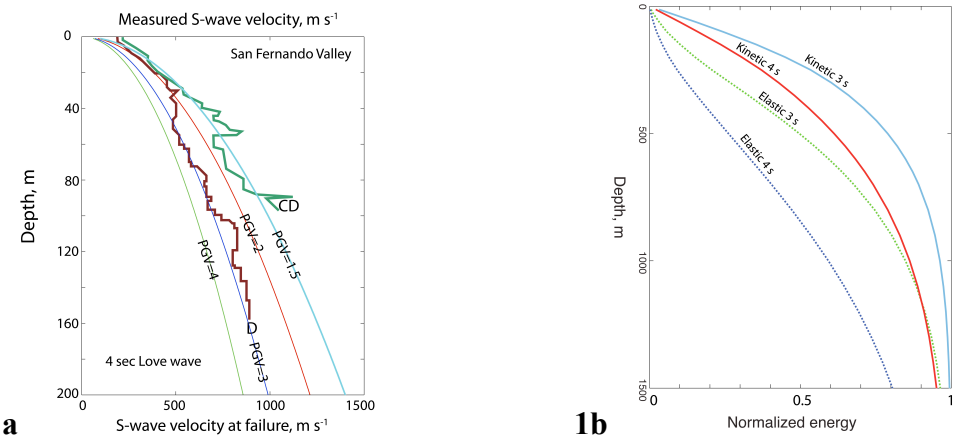

1a **1b**

Figure 1 (a) Averaged S-wave velocity for exhumed sediments (class CD [16]) and accumulating alluvium (class D [16]) in the San Fernando Valley [17]. Frictional failure in (1) at given particle velocity labeled in m/s occurs if the S-wave velocity is to the right of the smooth curves. Conservative parameters: $\mu_{\text{eff}} = 1$ (no fluid pressure), phase velocity 1500 m/s. Failure at given seismic velocity occurs at particle velocities to left of curve. San Fernando CD rocks follow a failure curve for 1.5 m/s particle velocity [12].

(b) Cumulative kinetic and elastic strain energies integrated over depth are equal for Love waves, here with periods of 3 and 4 s. Both energies are normalized to integrate to 1. Much of the energy resides in the upper kilometer and significant energy in the upper few 100 m. Such plots are the basis of our dimensional analysis of nonlinear attenuation. Modified from [18]. Site data from Whittier Narrows [19]; code from [20].

We continued our work on strong surface waves within sedimentary basins near Los Angeles by earthquakes on the San Andreas Fault [12,18], which are Love waves to the first order with likely periods of 3-4 sec [21-22]. Our methodology appraises the peak ground velocity (PGV) of these waves, but does not attempt to assess their period independently of [19,21-25]. Near-field velocity pulses from strike-slip faults are similar.

We have obtained a dimensional scaling for the attenuation of Love waves. The sum of kinetic and elastic strain energy per surface area is $W = \rho V_0^2 Z_L / 2$, where V_0 is peak velocity and energy is distributed over depth $Z_L \approx 1$ km in Fig. 1b. The dynamic strain is V_0 / c_L and the strain rate is $V_0 \omega / c_L$, where ω is angular frequency. Coulomb failure occurs above a depth $Z_{\text{dam}} = \beta^2(z) V_0 / c_L \mu_{\text{eff}} g$, which is 200-300 m using Fig. 1a. That is dissipation occurs over a significant part of the depth range is the Coulomb failure stress times the strain rate. The ratio of ambient energy per area to energy dissipation per area θ over a cycle with some algebra dimensionally yields the apparent quality factor Q

$$\frac{W}{\theta} = \left[\frac{1}{\omega}\right]\left[\frac{\pi c_L^3 Z_L g}{2\beta_{\text{dam}}^4}\right]\left[\frac{\mu_{\text{eff}}}{V_0}\right] \approx \frac{Q}{\omega} \quad , (7)$$

where the S-wave velocity at the base of the damaged layer is β_{dam}. The 1.5 m/s particle-

velocity waves as from a computed event on the San Andreas Fault [19,24] implies nonlinear attenuation. (2.5 m/s [25] is likely strongly nonlinear). The effective coefficient of friction and hence fluid pressure matter. Current hydrological data area available [e.g., 26-27]; the Los Angeles area is complicated in detail. Pre-industrial data are not precisely available but 1904 data is [28-32]. These data can be extrapolated to the time of the 1857 event; water table was likely near the surface or even artesian. The drawdown since 1957 is ~ 60 m in downtown Los Angeles [33]. Our scaling relationships indicate that the current velocity amplitude for nonlinear attenuation is ~10% greater than in 1857.

Intuitively, dynamic stress scales with dynamic velocity so nonlinear attenuation will tend to clip on velocity. Equations (5) and (6) are easily generalized to tensors in three-dimensions. The deviatoric stress tensor after (new) deformation is formally

$$\tau_{ij} = 2G\left[e_{ij}(U)\right] - 2G\varepsilon_{ij}(\text{old}) - 2G\Delta\varepsilon_{ij}(|\tau_{\text{new}}|), \quad (7); \quad \Delta\varepsilon_{ij}(|\tau_{\text{new}}|) \propto \left[e_{ij}(U)\right] - \varepsilon_{ij}(\text{old}), \quad (8)$$

where ij are tensor indicates, $e_{ij}(U)$ is the total deviatoric strain calculated from the displacement U, $\varepsilon_{ij}(\text{old})$ is the previous anelastic strain tensor. The absolute value $|\tau_{ij}(\text{new})|$ is proportional to the second invariant of the deviatoric stress tensor $\sqrt{\tau_{ij}\tau_{ij}}$ and may be normalized to give the shear stress in simple shear for use in (6). The tensor anelastic strain rate is proportional to the driving stress in (8). Vertical S-waves and Dr. Brittany Erickson (now UCSD) is helping with sophisticated numerical methods. Love waves do not change the mean stress [e.g., 34] and effective pressure $(\rho - \rho_w)gz$ represents its predictable value. In general, the mean stress $P \equiv \sigma_{ii}/3$ changes so $\tau_M = P\mu_M$ and $\tau_B = P\mu_B$ change. The flow law (6) is then analogous to Drucker-Prager plasticity [35], but attends to friction following changes in normal traction [e.g., 36-38].

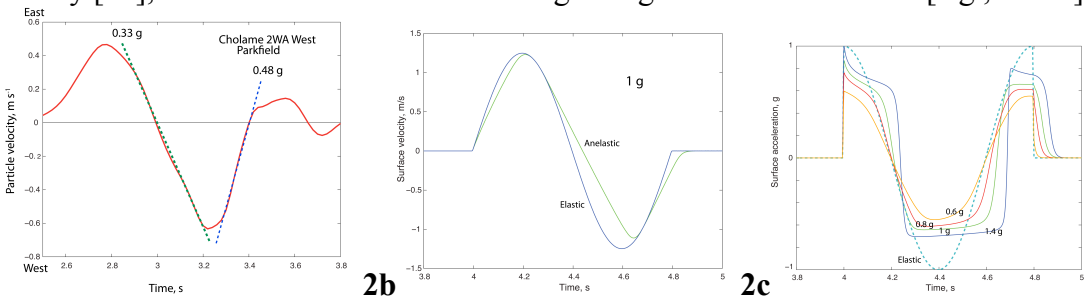

2a **2b** **2c**

Figure 2. (a) Observed particle velocity west component of Cholame 2WA for the 2004 Parkfield mainshock. Dashed lines show saw-toothed form of wave and sustained acceleration in g's, which provides estimates on the effective coefficient of friction in the subsurface. Modified from [39] using data from [40]. Zero time is arbitrary.
(b) Computed particle velocity at the surface. The incident elastic wave produces 1 g acceleration at the free surface. The anelastic waves experienced nonlinear attenuation in the shallow subsurface. They are saw-toothed. Note that the reflected wave's amplitude is more diminished than the surface amplitude. Zero time is arbitrary.
(c) Computed particle acceleration at the surface for nonlinear attenuated waves. Curves are labeled with the peak surface acceleration that the incident wave would produce in an elastic medium in g's. The incident elastic wave with 1 g acceleration is shown for reference. The duration of peak acceleration increases significantly with incident amplitude and the peak acceleration increases modestly. Zero time is arbitrary.

*[1] Sleep, N. H. (2012) Site resonance from strong ground motions at Lucerne, California, during the 1992 Landers Mainshock. *Bull. Seismol. Soc. Am.*, *102*(4), 1505–1513. *SCEC contribution number 1532.*

*[2] Sleep, N. H. (2013) Self-organization of elastic moduli in the rock above blind faults. *Geochem. Geophys. Geosyst.*, accepted. *SCEC contribution number 1693.*

[3] Fielding, E. J., Lundgren, P. R., Bürgmann, R. and Funning, G. J. (2009) Shallow fault-zone dilatancy recovery after the 2003 Bam earthquake in Iran, *Nature,* **458,** 64–68, doi:10.1038/nature07817

[4] Ribacchi, R. (2000) Mechanical tests on pervasively jointed rock material: insight into rock mass behaviour. *Rock Mech. Rock Eng.*, *33*(4), 243–266.

[5] Alejano, L.R. and Alonso, E. (2005) Considerations of the dilatancy angle in rocks and rock masses, *International Journal of Rock Mechanics Mining Sci.*, *42*(4), 481-507.

[6] Zhou, X. G., M. Cai (2010) A mobilized dilation angle model for rocks. *Int. J. Rock Mechanics Mining Sciences*, *47*, 368–384. doi:10.1016/j.ijrmms.2009.12.007

*[7] Sleep, N. H. (2012) Maintenance of permeable habitable subsurface environments by earthquakes and tidal stresses. *Int. J. Astrobiology*, *11*, pp 257-268, doi:10.1017/S1473550412000122. *SCEC contribution number 1674.*

*[8] Sleep, H. H. (2012) Constraint on the recurrence of great outer-rise earthquakes from seafloor bathymetry. *Earth Planets Space*, *64*, 1–2. *SCEC contribution number 1674.*

*[9] Sleep, N. H. (2012) Microscopic elasticity and rate and state friction evolution laws. *Geochem. Geophys. Geosyst.*, *13*, Q12002, doi:10.1029/2012GC004393. *SCEC contribution number 1680.*

[10] Nagata, K., M. Nakatani, and S. Yoshida (2012), A revised rate- and state-dependent friction law obtained by constraining constitutive and evolution laws separately with laboratory data, *J. Geophys. Res.*, *117*, B02314, doi:10.1029/2011JB008818.

[11] Ruina, A. (1983), Slip instability and state variable laws, *J. Geophys. Res*, *88*(B12), 10,359-10,370.

[12] Sleep, N. H. (2011), Seismically damaged regolith as self-organized fragile geological feature, *Geochem. Geophys. Geosyst.*, *12*, Q12013, doi:10.1029/2011GC003837. *SCEC contribution number 1515*.

[13] Yamada, M., J. Mori, and T. Heaton (2009) The slapdown phase in high-acceleration records of large earthquakes. *Seismol. Res. Lett.*, *80*(4), 559-564.

[14] Tobita, T., S. Iai, and T. Iwata (2010) Numerical analysis of near-field asymmetric vertical motion. Bull. Seismol. Soc. Am., 100(4), 1456–1469.

[15] Bradley, B. A., and M. Cubrinovski (2011) Near-source ground motions observed in the 22 February 2011 Christchurch earthquake. *Seismol. Res. Lett.*, *82*(6), 853-865.

[16] Magistrale, H., S. Day, R. W. Clayton, and R. Graves (2000) The SCEC Southern California reference three-dimensional seismic velocity model version 2. *Bull. Seismological Soc. Am.*, *90*(6B), S65–S76.

[17] Wills, C. J., M. Petersen, W. A. Bryant, M. Reichle, G. J. Saucedo, S. Tan, G. Taylor, and J. Treiman (2000) A site-conditions map for California based on geology and shear-wave velocity. *Bull. Seismological Soc. America*, *90*(6B), S187–S208.

[18] Sleep, N. H. (2010) Nonlinear Behavior of Strong Surface Waves Trapped in Sedimentary Basins. *Bull. Seismological Soc. Am.*, *100*, 826 - 832. *SCEC contribution number 1327.*

[19] Graves, R. W., B. T. Aagaard, K. W. Hudnut, L. M. Star, J. P. Stewart and T. H. Jordan (2008) Broadband simulations for Mw7.8 southern San Andreas earthquakes: Ground motion sensitivity to rupture speed, *Geophys. Res. Lett.*, *35*, L22302, doi:10.1029/2008GL035750.

[20] Herrmann, R. B. (2006). Computer Programs in Seismology, version 3.30, St. Louis University.

[21] Joyner, W. B. (2000) Strong motion from surface waves in deep sedimentary basins. *Bull. Seismol. Soc. Am.*, *90*(6B), S95-S112.

[22] Olsen, K. B., S. M. Day, J. B. Minster, Y. Cui, A. Chourasia, M. Faerman, R. Moore, P. Maechling, and T. Jordan (2006) Strong shaking in Los Angeles expected from southern San Andreas earthquake. *Geophys. Res. Lett. 33*, L07305, doi:10.1029/2005GL025472.

[23] Olsen, K. B., and 12 others (2009) ShakeOut-D: Ground motion estimates using an ensemble of large earthquakes on the southern San Andreas fault with spontaneous rupture propagation, *Geophys. Res. Lett.*, *36*, L04303, doi: 10.1029/2008GL036832.

[24] Graves, R. (1996) Simulating seismic wave propagation in 3D elastic media using staggered grid finite differences. *Bull. Seismol. Soc. Am.*, *86*, 1091–1106.

[25] Graves, R. W., Aagaard, B. T., and Hudnut, K. W. (2011) The ShakeOut earthquake source and ground motion simulations. *Earthquake Spectra*, *27*, 273-291; doi:10.1193/1.3570677

[26] Reichard, E. G., et al. (2003) Geohydrology, Geochemistry, and Ground-Water Simulation-Optimization of the Central and West Coast Basins, Los Angeles County, California. U.S.G.S Water-Resources Investigations Report 03-4065, 184 pp.

[27] Metropolitan Water District of Southern California (2007) Chapter IV – Groundwater basin reports San Fernando Valley basins - Upper Los Angeles River area basins. in Final Groundwater Assessment Study A Status Report on the Use of Groundwater in the Service Area of the Metropolitan Water District of Southern California Report Number 1308, pp. IV-2-1-IV-2-19.

[28] Mendenhall, W. C. (1905a) Development of underground waters in the central costal plain region of southern California, USGS Water Supply and Irrigation Paper 138, 162 pp.

[29] Mendenhall, W. C. (1905b) Development of underground waters in the western costal plain region of southern California, USGS Water Supply and Irrigation Paper 139, 103 pp.

[30] Mendenhall, W. C. (1905c) Development of underground waters in the eastern costal plain region of southern California, USGS Water Supply and Irrigation Paper 137, 140 pp.

[31] Mendenhall, W. C. (1905d) The hydrology of San Bernadino Valley, California, USGS Water Supply and Irrigation Paper 142, 124 pp.

[32] Mendenhall, W. C. (1908) Ground waters and irrigation enterprises in the foothill belt of southern California, USGS Water Supply 219, 175 pp.

[33] Johnson, T., and B. Chong (2005) A century of groundwater changes in the central and west coast basins. Water Replenishment District of Southern California, Techical Bulletin, vol. 4, summer, 2 pp.

[34] Bullen, K. E., and B. A. Bolt (1985) *An Introduction to the Theory of Seismology, 4th ed*., Cambridge University Press, Cambridge, 499 pp.

[35] Drucker, D. C., and W. Prager (1952), Soil mechanics and plastic analysis or limit design, *Q. Appl. Math.*, *10*, 157–165.

[36] Linker, M. F., and J. H. Dieterich (1992) Effects of variable normal traction on rock friction: Observations and constitutive equations, *J. Geophys. Res.*, *97*(B4), 4923-4940.

[37] Perfettini, H., J. Schmittbuhl, J. R. Rice, and M. Cocco, (2001), Frictional response induced by time-dependent fluctuations of the normal load, *J. Geophys. Res.*, *106*(9B7) 13,455-13,472.

[38] Kilgore, B., J. Lazos, N. Beeler, and D. Olgesby (2012) Laboratory observations of fault strength in response to changes in normal stress. *J. Applied Mech.*, *79*, 031007.

[39] Sleep, N. H., and P. Hagin (2008), Nonlinear attenuation and rock damage during strong seismic ground motions, *Geochem. Geophys. Geosyst.*, *9*, Q10015, doi:10.1029/2008GC002045. *SCEC contribution number 1217.*

[40] Shakal, A. F., H. R. Haddadi, V. Graizer, K. Lin, and M. Huang (2006) Some key features of the strong-motion data from the **M** 6.0 Parkfield, California, earthquake of 28 September 2004, *Bull. Seismol. Soc. Am., 96*, S90-S118.

* Works during this grant period.